Constraints on age and construction process of the Foundation chain submarine volcanoes from magnetic modeling

Marcia Maia, Jérôme Dyment, David Jouannetaud

Constraints on age and construction process of the Foundation chain submarine volcanoes from magnetic modeling

Marcia Maia [a], Jérôme Dyment [b], David Jouannetaud [a]

a CNRS UMR 6538 Domaines Océaniques, IUEM, Université de Bretagne Occidentale, 1 place Nicolas Copernic, 29280 Plouzané, France

b CNRS UMR 7097 Laboratoire de Géosciences Marines, IPGP, 4 place Jussieu, 75005 Paris, France

Abstract

The interaction between the Foundation hotspot and the Pacific–Antarctic Ridge (South Pacific) is one of the two known cases where a ridge is approaching a hotspot. This ridge–hotspot relative movement results in a change in the morphology of the volcanoes along the chain as the age of the lithosphere at the time of edifice formation progressively diminishes. Four hundred kilometers west of the Pacific–Antarctic Ridge axis, volcanism is distributed along two sub-parallel lines of volcanoes, separated by distances diminishing from ~100 km at the west to ~50 km near the axis of the ridge. The magnetic anomalies mapped on this part of the chain show a pattern clearly dominated by the magnetic signature of the seamounts. The anomalies were forward modeled using a remanent magnetization of normal or reversed polarity within the volcano topography. The resulting pattern of normal and reversed magnetization is consistent with the intervals of the geomagnetic polarity time scale for the last 5 Ma, the age of the oldest studied volcano. These magnetic anomalies therefore represent an independent means of dating the volcanic edifices. The ages deduced from the modeling are consistent with the hypothesis of volcanoes built by a hotspot on the fast moving Pacific plate and are in good agreement with the published radiometric dates, although these dates tend to correspond to the late constructional stages of the edifices. The differences between magnetic and radiometric ages suggest that the average time span to build a volcano of the Foundation chain is about 1 million years, in agreement with other intraplate edifices. The difference between the magnetic ages of the seamounts and of the underlying crust, both deduced from the magnetic anomaly analysis, show that the ridge has approached the hotspot at a rate of 40 km/Ma.

1. Introduction

Seamount magnetism has often been used to deter- mine paleomagnetic poles and constitute one of the main bodies of data available for the study of the apparent polar wander path of oceanic plates, especially for the Pacific plate (e.g. [1–12]). The magnetic modeling of seamounts is a complex procedure, mainly because rock magnetization can be acquired in different ways and modified by the alteration processes triggered by hydrothermal circulation, acting for long times after the seamount formation [13–15]. One of the fundamental assumptions made in such paleomagnetic studies is that the magnetic anomaly is dominated by the effect of remanent magnetization, and therefore reflects the magnetic field at the time

of the construction of the edifice. However, viscous remanent magnetization and induced magnetization can also contribute to up to 15–25% of the total signal, although this part of the anomaly would be largely due to intrusives [15]. The long time span involved in the formation of the largest edifices (e.g. [16]) can also further complicate the modeling, especially if the edifice was built during a period of frequent magnetic field reversals.

The magnetic signature of intraplate volcanoes may also be useful to determine their ages. Ar40 – Ar39 methods, although essential to establish sea- mount ages, face the problem that many of the samples, obtained by dredging, are only representative of the latest volcanic events. The construction of the smaller intraplate volcanoes can be a fast process and the main body of most volcanoes is probably built in less than 1 my [17]. Longer time spans may be associated with the largest edifices [16]. By com- paring magnetic models of seamounts with their argon ages, one may obtain insights on the structure of the edifice and on the history of edifice formation [7,18].

In January–February 1997, R/V L'Atalante acquired multibeam bathymetry and scalar surface magnetic data over the zone of interaction between the Foundation hotspot and the Pacific–Antarctic Ridge (PAR) (Figs. 1 and 2). Ship tracks are oriented N128E, perpendicular to the average direction of the volcanic structures. In addition, a profile located south of the area, away from the volcanoes, was run along a theoretical flow line to provide reliable seafloor spreading magnetic anomaly identifications (Fig. 2). The track spacing of 9 to 15 km was chosen such as to insure a slight overlap of the bathymetry swaths at average seafloor depths and is too large to allow detailed magnetic study of the individual volcanoes. Although the sparse magnetic data constitutes a challenge, a forward modeling approach focused on individual seamounts can provide some useful constraints on the magnetic polarity of the edifices. Predicted sea surface magnetic anomaly can be modeled for every single isolated edifice assuming a uniform magnetization and using the well-constrained bathymetry, then compared to the observed signal to deter- mine (1) whether a uniform polarity is compatible with the data and (2) in favorable cases, what the seamount polarity is. Such an approach benefits from the north–south direction of the profiles, which optimally record the polarity signal of young magnetized bodies.

In this paper we apply such a technique to model the magnetic anomalies associated with the young volcanoes of the Foundation chain, in the South Pacific Ocean, where a good knowledge on the argon ages is also available [19,20]. Gravity models [21] and a geodynamic study [22] have addressed the geologic history of the chain and provide background information for the magnetic models.

2. Geodynamic setting of the Foundation chain

The Foundation chain (Fig. 1) was formed by the passage of the Pacific plate over the Foundation hot- spot. Volcano ages decrease progressively to the east, from 21 my to very recent ages for the edifices located near the PAR axis [19,20]. The basalt composition of the volcanoes from the main body of the chain (1248W–1158W, see Fig. 1) shows enrichment similar to other hotspot-derived intraplate volcanoes [24–27]. About 400 km away from the PAR axis (near 1208W) the morphology and the chemical composition of the volcanoes change as the result of the interaction between the Foundation hotspot and the ridge. The chain separates in two roughly parallel lines (Fig. 2), the North system and the South system. In both

systems the volcanoes are mainly grouped into ridges. A systematic change in the morphology of the edifices is observed from west to east. The westernmost ridges are formed by tall volcanoes, sometimes reaching depths of less than 400 m, whereas near the PAR the ridges are formed by smaller, flat topped edifices with summit calderas, which coalesce and form quasi-continuous features. The elongated morphology of most of the edifices of the South system is suggestive of fissure volcanism and of emplacement along lithospheric cracks. The South system is interpreted as a secondary volcanic line, which formed on top of the flexural arch created in response to the load of the north volcanic system [21,22].

Published radiometric ages show that the chain obeys roughly a theoretical hotspot age–distance trend with younger ages towards the southeast [19,20] where the hotspot is presently located [22]. Detailed sampling of the small dome-shaped edifices near the PAR reveal that the age pattern displays some irregularity [20]. This can be interpreted as resulting from emplacement of the volcanoes controlled by flexural and thermal stresses acting in the plate, as suggested by Hieronymus and Bercovicci [28]. The youngest end of the Foundation chain appears to be a good example of the partial control of the mechanical properties of the plate on the surface distribution and on the morphology of hotspot volcanoes.

3. Data and method

Multibeam bathymetry is homogeneous over the whole area, allowing the calculation of a detailed grid. For the purposes of this study a grid interval of 400 m was adopted. The data were processed and gridded using a near-neighbor gridding algorithm. Magnetic data were acquired with a surface proton magnetometer at a sampling rate of 20 s (100 m at a ship speed of 10 knots). The total field measurements were reduced to anomalies by removing the International Geomagnetic Reference Field models (IGRF) [29] interpolated for year 1997. Spurious data related to dredge operations and spikes were removed and the clean data set was filtered with a median filter over 5 to 20 points (depending on the noise level) and interpolated to a 1-min interval.

3.1. Magnetic modeling

The magnetic effect of a constant thickness layer with laterally variable magnetization is given by [30–32]

$$\mathbf{F}[\Delta T(x,y)] = \mathbf{F}[M(x,y)]\{\mu_0\theta_m\theta_f \exp^{|k|z_0}(\exp^{|k|z_1} - \exp^{|k|z_2})/2\} \quad (1)$$

where F is the Fourier transform, $\Delta T(x,y)$ is the magnetic anomaly computed at a depth z_0, M(x,y) is the magnetization of the layer between depths z_1 and z_2, $z_1 < z_2$, μ_0 is the magnetic permeability in vacuum, k_x and k_y are wave numbers in the x and y directions with

$$|k| = (k_x^2 + k_y^2)^{1/2},$$

And

$$\theta_{\mathbf{m}} = \mathbf{m}_z + i(\mathbf{m}_x k_x + \mathbf{m}_y k_y)/|k|$$

$\theta_f = \mathbf{f}_z + i(\mathbf{f}_x k_x + \mathbf{f}_y k_y)/|k|$

where $I = (-1)^{1/2}$ and unit vectors **f** and **m** give the orientations of the regional field and the magnetization, respectively.

In order to compute the magnetic anomaly of the seamounts, the bathymetric grid is cut into several layers 100 m thick. For each layer a value of "1" (respectively "0") is assigned to grid points with "rock" (respectively without "rock"). The choice of such thin layers allows us to separate the seamounts from the underlying seafloor. The subsidence of the seafloor is corrected using a $(t)^{1/2}$ law [33], yielding a residual bathymetry grid with an average depth of 3160 m. After visual examination of the residual bathymetry, a value of 2800 m is chosen to define the base of the edifices. This means that only depths shallower than 2800 m are considered in the calculation. Most of the edifices are conveniently modeled with this approach and only the biggest volcanoes are slightly truncated at their bases. Calculations run with a deeper basal value (3100 m), closer to the grid average, show that the truncation does not significantly alter the final result. This procedure avoids considering in the same models the magnetic effects of the seamounts and of the oceanic crust, the latter being modeled separately. Volcanic crustal roots are not included in the model, since no good constraint from seismic data is available, although gravity models suggest thickened crust below the larger volcanoes of the North system [21]. If a local compensation model is to be expected, our approach would consistently overestimate the magnetization intensity in the layers considered for calculation, to compensate for the effect of the volcanic roots, but it would certainly not affect the polarity of the magnetization required to fit the shape of the observed anomalies. These deeper effects are probably of smaller amplitude because (1) the sources are further away from the magnetometer and (2) the deeper crust magnetization is lower than the near-surface one (e.g. [34]).

Once the source geometry is defined, the magnetization direction, polarity and intensity have to be set. A magnetization intensity of 10 A/m is adopted, which represents the higher range of recent mid- ocean ridge extrusive basalt magnetization (see [34], for a review). Basalt erupted in the vicinity of hotspots exhibits a higher Fe and Ti content as a result of higher pressure of melting, hence a stronger magnetization (e.g. [35]). The magnetization polarity is modeled by grids with values of +- 1 reproducing the normal and reverse polarities For each layer of the geometrical grid extracted from the bathymetric grid, the magnetization intensity and the magnetization polarity grid are multiplied to obtain the magnetization grid required in the calculations (Eq. (1)). We assume a vertically uniform magnetization, which (1) does not take into account the various magnetization intensities of different crustal layers (e.g. [34]) and (2) may average changes on the direction of the magnetization related to field reversals in the piled lava flows. Depth-varying magnetization intensity of uniform polarity would certainly not hamper the final result as long as the sign of the anomaly is considered. Depth-varying magnetization polarity may lead either to neglect shorter polarity intervals, meaning that the resolution of this technique is limited by the duration of volcanic edifice formation, or to a complex anomaly, which cannot be–and is not–further interpreted with the available data. The regional field vector is supposed parallel to the present-day geomagnetic field given by the IGRF models, and the magnetization vector parallel to the latitude-dependent axial dipolar field. The complete bathymetric coverage of the study area allows a fully three-

dimensional calculation of the magnetic anomalies. A magnetic anomaly grid is computed for each constant thickness layer and the total computed magnetic anomaly grid is given by the sum of the computed anomalies for all layers. Due to the relatively wide ship track spacing (9 to 15 km), it was meaningless to build an observed magnetic anomaly grid from the available observations. Instead we extracted magnetic anomalies from the computed anomaly grid along the real ship tracks to allow the comparison between modeled and observed anomalies. The sign and shape of both anomalies were visually compared for each volcano or volcanic ridge. We did not attempt to exactly model the shape and amplitude of the anomaly for each volcano. This would require a detailed structural model for each edifice and a much larger magnetic data set than what is available, each volcano being often crossed by only one or two parallel profiles. Our main objective is to estimate for each volcano whether it was mainly built during a normal or a reversed polarity period.

3.2. Seafloor spreading magnetic anomalies

In order to improve the quality of the fit between the observed and modeled magnetic anomalies, the magnetic anomalies due to the underlying oceanic crust should be considered as well, although their amplitudes are considerably smaller than those related to the volcanoes. Seafloor spreading anomaly crossings are identified on all available magnetic anomaly profiles (Fig. 3a), including Profile 1 (along a "flow line", see Fig. 2 for location) and the short turning profiles between the main lines, complemented by other magnetic anomaly profiles obtained from the GEODAS data base [NGDC, 2001]. These interpreta- tions are confirmed by the long-wavelength positive or negative anomalies observed on the N12°E profiles. The isochrons defined from the magnetic anomaly identifications are further interpolated to compute an age grid (Fig. 3b). The age values range from 10 my (anomaly 5) in the northwestern corner of the area to zero along the Pacific–Antarctic ridge axis. Magnetic polarities are ascribed depending on the age, following Cande and Kent [36] geomagnetic polarity time scale (Fig. 3c). A magnetization intensity of 10 A/m is considered at the ridge axis and decreases progressively with the age of the crust, allowing for rock alteration and the associated change in magnetization resulting from the transformation of titanomagnetite to titanomaghemites [37–41]. Surprisingly enough, a better agreement between synthetic anomalies and Profile 1 is obtained for a $(t)^{1/2}$ relationship between magnetization intensity and age, although an exponential relationship is generally favored in other studies [42–44]. The seafloor spreading magnetic anomalies are modeled assuming a magnetic layer 500 m thick. A depth–age grid reproducing the subsidence observed in the study area is used as the top of this layer. Fig. 4 shows a comparison between observed and modeled anomalies along Profile 1. The synthetic magnetic anomalies associated to the underlying oceanic crust are removed from the observed magnetic anomalies. The residuals can therefore be directly compared with results from the modeling of seamount magnetic anomalies.

3.3. Magnetic anomalies associated with the volcanoes

In our calculations, we consider the two simple cases of either normal or reversed uniform seamount magnetization. Modeled anomalies for the two cases are compared to the observed ones (corrected for the magnetic effect of the underlying oceanic crust) and a correlation coefficient is calculated over windows corresponding to each seamount (Fig. 5). By selecting the case (normal or reversed) that better describe the observed anomaly for each seamount,

we construct a polarity model for the whole area (Fig. 6a). This final magnetic model is composed of purely normal, purely reversed, and mixed polarity magnetized bodies corresponding to each edifice. The fit quality is evaluated in three classes: good, fair, and poor fit. The first class corresponds to volcanoes of a clearly defined polarity, either normal or reverse, the second class corresponds to edifices showing a dominant polarity and the third class corresponds to edifices where the calculated anomaly produces a poor fit to observed anomaly. Further refinements could be added to the polarity structures presented in Fig. 6a. It should be remembered, however, that our purpose was not to achieve a perfect fit of the magnetic anomaly amplitude for each volcano but rather to determine the magnetic polarity of each seamount.

In Fig. 7 we compare the observed signal and the anomalies calculated using the polarity model displayed in Fig. 6a along each profile. As expected from the correlation coefficients (Fig. 5), the fit is very good for the edifices near the PAR axis (Profiles 2 to 4). Further west, the fit quality decreases for the larger volcanoes. The shape of the observed anomaly is roughly reproduced by our model but the calculated anomaly is often narrower and of a smaller amplitude than the observed one. Generally, the model reproduces the long wavelength of the anomaly but is unable to account for shorter wavelengths superimposed on the signal. This probably reflects additional complexity in the magnetic structure of the volcanoes. The fit between the observed and modeled anomalies is generally better for the South system and the dome-shaped volcanoes than for most edifices of the North system, suggesting complexities in the magnetic structure of the latter that cannot be easily reproduced by any simple modeling effort. Such a difference in the magnetic structure of the volcanoes may be related to different formation processes for the North and South systems. The South system probably formed along fissures on top of the flexural arch resulting from the emplacement of the North system volcanoes [21]. In the North system volcanoes the magmatic activity may have lasted for longer periods, although the main (shield) building phase may be roughly equivalent for the edifices of the north and the south.

4. Results and discussion

Despite limitations of the simple magnetic models used here, the distribution of magnetic polarity deduced from the analysis of the magnetic anomalies present significant trends. East of 111°30’W, all seamounts are normally magnetized, as it should be expected for volcanoes built during the Brunhes magnetic period. Further west, bands of alternating pola- rities are observed, as, for example, reversed polarity at 114°30’W or normal polarity at 113°20’W. This succession resembles the sequence of geomagnetic polarity for the last 5 million years. Discrepancies may arise mainly from two different causes. The first is that the volcanoes were not necessarily built following a regular age progression. Since lithospheric control on the emplacement of the edifices has been demonstrated, the expected age progression may deviate from the linear trend of an ideal hot spot model. However, the geodynamic and age studies of the Foundation chain showed that for this long linear chain, the age progression holds in a regional scale, with relatively localized irregularities [19,20,22].

The second cause is that construction of a volcanic edifice spans finite length of time that is often longer than the shorter polarity intervals or which may cross boundaries between intervals. This second point can be addressed by tentatively simulating the observable polarity

sequence for different lengths of construction of the volcanic edifices. This can be done by convolving the polarity scale with a filter simulating the construction of a volcano. The filter was designed based on estimations of the length of the building stages and of eruptive rates made for the Society hot- spot [45], which is more comparable to the Founda- tion chain than Hawaii. The filter reproduces the fast building of the main shield with strong eruptive rates followed by a less magmatic and shorter post-shield phase and is a rough simplification of the complex stages of the building of an intraplate volcano. In order to account for the varying dimensions of the volcanoes of the studied area, three cases were con- sidered. The first considers a very fast building (200000 yr), the second an intermediate building (400 000 yr) and the third a long construction phase (800000 yr). The filters are displayed in Fig. 8. The result of the operation is a smoother polarity sequence, the longest construction period corresponding to the smoothest sequence (Fig. 6a). In this case, only the longer polarity periods (Brunhes = anomaly 1, Matuyama, Gauss = anomaly 2A, Gilbert, anomaly 3) are distinguished. If the construction period is short, the smaller polarity periods such as the Olduvai (= anomaly 2) and Jaramillo events will appear. The comparison of the filtered sequences with the polarity of the volcanoes inferred from the magnetic anomalies (Fig. 6a) suggests a short construction period for the small dome-shaped edifices located near 112°W, formed around 1 Ma (Jaramillo). The younger volcanoes closer to the PAR axis show an homogeneous polarity corresponding to the Brunhes period. The bigger edifices located west of 113°W were probably built over longer periods since the short polarity episodes of anomalies 2A and 3A cannot be systematically identified. This is true for both the circular edifices of the North system and for the elongated volcanoes of the South system.

We can reasonably consider that the systematic trends observed in the magnetic polarity deduced from our analysis of the magnetic anomalies associated to the seamount indeed represent variations related to the age progression of the seamounts. The observed pattern of seamount polarity is unlikely to arise unless the eruption periods are shorter than the longer geomagnetic polarity intervals and the ages follow a quite regular progression. Much longer eruption periods would increase significantly the number of volcanoes displaying a mixed polarity. A complex, irregular age distribution would result in a less coherent polarity pattern. The magnetic polarity can therefore be used as a tool to estimate the age of the seamounts, with a resolution of 1 Ma or less depending on the area, the duration of formation and the reversal frequency. Based on Fig. 6a, we have applied this technique to convert the magnetic polarity distribution into age intervals using the geomagnetic scale of Cande and Kent [36]. These age intervals are named “magnetic ages” hereafter (Fig. 6b).

Ages are easily ascribed on the eastern part, where the Brunhes period (anomaly 1: 0–0.78 Ma), the younger part of the Matuyama period (anomaly 1: 0.78–0.99 Ma), the Jaramillo event (anomaly 1: 0.99–1.07 Ma) and the mid-part of the Matuyama period (anomaly 1: 1.07–1.77 Ma) are easily recognized. The ages of the Olduvai event (anomaly 2: 1.77–1.95 Ma) and the older part of the Matuyama period (anomaly 2: 1.95–2.58 Ma) are given to sea- mounts of the South system (seamount Platon and an unnamed linear volcano), where the polarity sequence is clear, although no age is ascribed to the corresponding part of the North system due to poor model fit (seamount Newton). Further west, age of the Gauss period (anomaly 2A: 2.58–3.58 Ma) is given to sea- mount Wegener on the Southern system, although age ranges of 2.58–3.04 Ma (2A.1n, Mercator seamount), 3.04–3.33 Ma; and 3.33–3.58 Ma (2A.3n, Mendeleiev seamount) are ascribed to seamounts of the North system. The correlation coefficient (Fig. 5)

suggests that the polarity for the unnamed volcano corresponding to the time interval 3.04–3.33 Ma is dominantly, but not purely reversed, in agreement with the polarity time scale for this period. The long reversed interval between anomalies 2A and 3 is well marked on the interpreted seamount polarities, and an age range of 3.58–4.62 Ma is given to these areas (Mohorovicic seamount, part of Mendel seamount and of Linné Ridge) to reflect the possible effect of long emplacement duration, as suggested by Fig. 6a (lower line). Finally the age of anomaly 3 (4.18–4.89 Ma) is ascribed to the westernmost seamounts, including Linné seamount.

4.1. Comparison between magnetic and radiometric ages

Fig. 9 shows a comparison of published radio- metric ages [19,20] and our magnetic ages. The agreement between the magnetic and radiometric ages is in general good. It is usually better for the young volcanoes (younger than 1 Ma) that have a fast and simple building history, as inferred from both the young radio- metric ages and the dome morphology. For older vol-canoes, and especially those of the South system, most radiometric ages tend to lie in the younger range of the magnetic age intervals, as it should be expected for rocks collected at the seamount summits, which represent the latest constructional period.

The magnetic anomaly of a volcano integrates the effect of the magnetization of all the rocks constitutive of this volcano. Therefore, the average magnetization obtained through our analysis is mostly representative of the main constructional phase of the edifice rather than of any later volcanic episode. The fact that many volcanoes show a clear polarity indicates that they formed fast enough to span a single polarity interval. The recent geomagnetic polarity intervals are roughly 1 my long; this is consistent with estimated durations of the main constructional phase of the bigger volcanoes. The young smaller volcanoes built during the Brunhes period were probably built much faster, as their radiometric ages indicate, but the lack of short reversals prevents to better constraint this point. Only the small volcanoes formed during the short reversals around Jaramillo (Pauling, Pascal, Schrödinger, see Figs. 2, 6a and 6b) can be said to have constructional phases probably shorter than 1 Ma. The differences between radiometric and magnetic ages seem to con- firm that the magnetic ages date the older main constructional phase, whereas the radiometric ages of dredge samples coming from volcano summits or upper flank waste reflect the last stages of the volcanic construction. Mohorovicic volcano, where radiometric dating indicates a long period of activity (2.8 my), may be similar to Jasper seamount [16], where a 7 my activity interval was reported. For Mohorovicic volcano, there is a good agreement between the younger edge of the magnetic age interval and the older radio- metric age. Two younger radiometric ages may correspond to later magmatic phases that do not significantly contribute to the building of the main edifice.

4.2. Ridge–hotspot relative motion

A good additional test for the consistency of our dating method is the comparison of the ridge–hotspot relative motion between the PAR and the Foundation hotspot deduced from the magnetic ages with existing models based on global plate kinematics and hotspot tracks (e.g. [46,47]). Accordingly, we first computed the age of the plate at the time of each volcano formation (i.e. the age of loading) by subtracting the age of the volcano from the age of the

underlying crust. This value is multiplied by the half-spreading rate, which remained relatively constant at 47 km/Ma through the last 5 my, to yield the distance between the hotspot and the ridge at the time of the volcano formation. The results are shown in Fig. 10, with only the average magnetic age of each volcano being considered for simplicity. Although the scatter is high, a linear regression fit yields a speed of about 40 km/Ma for the motion of the PAR with respect to the Foundation hotspot (green line), slower but in reasonable agreement with the theoretical value of 43 km/Ma (red line; [46–48]). The predicted hotspot location is roughly 20 km away from the ridge, in agreement with previous works [22].

5. Summary and conclusion

The magnetic anomalies collected across the Foundation Seamount chain are dominated by the signature associated to the seamounts, and are successfully modeled by remanent magnetization of normal or reversed polarities within the anomalous topography. The distribution of normal and reversed magnetization presents a consistent pattern which resembles intervals of the geomagnetic polarity time scale for the last 5 Ma. These magnetic anomalies therefore represent an independent mean to date the volcanic edifices of the Foundation Seamount chain. The ages deduced from the magnetic anomaly modeling are consistent with the hypothesis of volcanoes built by a hotspot on the fast moving Pacific plate. They are in good agreement with the published radiometric dating, which appear to correspond to the latter constructional stages of the edifices. The average time span to build a large volcano of the Foundation chain is about 1 million years, in agreement with other intraplate edifices, while the smaller edifices appear to form faster. The difference between the ages of the seamounts and of the under- lying crust, both deduced from the magnetic anomaly analysis, shows that the ridge gets progressively closer to the hotspot at a rate of 40 km/Ma.

Beyond the classical use of Vine–Matthews anomalies to date normal oceanic crust, marine magnetic anomalies appear therefore as a tool to date more complex features such as linear volcanic chains. From our study, it can be expected that cross-chain magnetic surveys of hotspot track volcanoes would provide valuable data in terms of the volcanic built up and the hotspot history—possibly the unbiased data which have been missing so far to carefully evaluate the hypothesis of fixed hotspots and, in fine, address their nature?

Acknowledgements

The authors would like to thank P. Gente, who helped with the bathymetry data. We also thank C. Devey for kindly providing the multibeam data from the Sonne 100 cruise to complete our data set. Discussions with J. Arkani-Hamed during the early steps of this work were essential to the development of the model technique. Careful reviews made by W. Sager, J. Arkani-Hamed and P. Patriat significantly improved the present paper. Several figures were drawn using the GMT Software [49]. This study was funded by CNRS-INSU through the “Océans” program. These are contribution nos. 945 of IUEM, European Institute for Marine Studies (Brest, France) and 2046 of IPGP.

References

[1] B.F. Grossling, Seamount magnetism, in: M.N. Hill (Ed.), The Sea—Ideas and Observations on Progress in the Study of the Seas. Vol. 4: New Concepts of Sea Floor Evolution, Part I: General Observations, John Wiley and Sons, MN, 1970, pp. 129 – 155.
[2] R.L. Parker, The determination of seamount magnetism, Geophys. J. R. Astron. Soc. 24 (1971) 321 – 324.
[3] C.G.A. Harrison, R.D. Jarrard, V. Vacquier, R.L. Larson, Paleomagnetism of Cretaceous Pacific seamounts, Geophys. J. R. Astron. Soc. 42 (1975) 859 – 882.
[4] Z. Ben-Avraham, C.G.A. Harrison, E. Klein, Y. Shoham, Seamount magnetism in the Ionian Sea, eastern Mediterranean, Mar. Geophys. Res. 5 (1983) 389 – 404.
[5] J.A. Hildebrand, R.L. Parker, Paleomagnetism Cretaceous Pacific seamounts revisited, J. Geophys. Res. 92 (1987) 12695 – 12712.
[6] R.L. Parker, L. Shure, J. Hildebrand, The application of inverse theory to seamount magnetism, Rev. Geophys. 25 (1987) 17 – 40.
[7] W. Sager, M.S. Pringle, Paleomagnetic constraints on the origin and evolution of the Musicians and South Hawaiian seamounts, Central Pacific Ocean, in: B.H. Keating, P. Fryer, R. Batiza, W. Boehlert (Eds.), Seamounts, Islands and Atolls, Geophysical Monograph, vol. 43, American Geophysical Union, Washington, DC, 1987.
[8] W. Sager, M.S. Pringle, Mid-Cretaceous to early Tertiary apparent polar wander path of the Pacific plate, J. Geophys. Res. 93 (1988) 11753 – 11771.
[9] R.L. Parker, A statistical theory of seamount J. Geophys. Res. 93 (1988) 3105 – 3115.
magnetism,
[10] R.L. Parker, A theory of ideal bodies for seamount magnetism, J. Geophys. Res. 96 (1991) 16101 – 16112.
[11] D.C.P. Masalu, K. Tamaki, W.W. Sager, Paleomagnetism of the Joban Seamount Chain: its origin and tectonic implications for the Pacific plate, J. Geophys. Res. 102 (1997) 5145 – 5155.
[12] W.W. Sager, A.A.P. Koppers, Late Cretaceous polar wander of the Pacific plate: evidence of a rapid true polar wander event, Science 287 (2000) 455 – 459.
[13] J. Gee, L. Tauxe, J. Hildebrand, H. Staudigel, P. Lonsdale, Non-uniform magnetization of Jasper Seamount, J. Geophys. Res. 93 (1988) 12159 – 12175.
[14] J. Gee, H. Staudigel, L. Tauxe, Seamount magnetization, Nature 342 (1989) 170 – 173.
[15] J. Gee, H. Staudigel, L. Tauxe, T. Pick, Y. Gallet, Magnetization of the La Palma Seamount Series: implications for seamount paleopoles, J. Geophys. Res. 98 (1993) 11743 – 11768.
[16] M.S. Pringle, H. Staudigel, J. Gee, Jasper Seamount: seven million years of volcanism, Geology 19 (1991) 364 – 368.
[17] E.D. Jackson, E.A. Silver, G.B. Dalrymple, Hawaiian– Emperor chain and its relations to Cenozoic Pacific tectonics, Geol. Soc. Amer. Bull. 83 (1972) 601–618.
[18] W.W. Sager, R.A. Duncan, D.W. Handschumacher, Paleo- magnetism of the Japanese and Marcus–Wake Seamounts, Western Pacific ocean, in: M.S. Pringle, W.W. Sager, W.V. Silter, S. Stein (Eds.), The Mesozoic Pacific: Geology, Tec- tonics and Volcanism, Geophysical Monograph, vol. 77, American Geophysical Union, Washington, DC, 1993.
[19] J. O'Connor, P. Stoffers, J.R. Wijbrans, Migration rate of volcanism along the Foundation chain, SE Pacific, Earth Planet. Sci. Lett. 164 (1998) 41 – 59.
[20] J. O'Connor, P. Stoffers, J.R. Wijbrans, En echelon volcanic elongate ridges connecting intraplate Foundation Chain volcanism to the Pacific–Antarctic spreading center, Earth Planet. Sci. Lett. 189 (2001) 93 – 102.
[21] M. Maia, J. Arkani-Hamed, The support mechanism of the young Foundation seamounts inferred from bathymetry and gravity, Geophys. J. Int. 149 (2002) 190 – 210.

[22] M. Maia, C. Hémond, P. Gente, Contrasted interactions between plume, upper mantle and lithosphere: the Foundation Chain case, Geophys. Geochem. Geosyst. 2 (2001) (paper number 2000GC000117).
[23] W.H.F. Smith, D.T. Sandwell, Global sea floor topography from satellite altimetry and ship depth soundings, Science 277 (1997) 1956 – 1962.
[24] C. Hémond, C.W. Devey, The Foundation Seamount Chain, Southeast Pacific: first isotopic evidence of a newly discovered hotspot track, J. Conf. Abstr. (Goldschmidt, Heidelberg) 1 (1996) 255.
[25] C.W. Devey, R. Hékinian, D. Ackermand, N. Binard, B. Francke, C. Hémond, V. Kapsimalis, S. Lorenc, M. Maia, H. Möller, K. Perrot, J. Pracht, T. Rogers, K. Statteger, S. Steinke, P. Victor, The Foundation Seamount Chain: a first survey and sampling, Mar. Geol. 137 (1997) 191 – 200.
[26] R. Hékinian, P. Stoffers, C.W. Devey, D. Ackermand, C. Hémond, J. O'Connor, N. Binard, M. Maia, Intraplate versus oceanic ridge volcanism on the Pacific Antarctic Ridge near 378S–1118W, J. Geophys. Res. 102 (1997) 12265 – 12286.
[27] R. Hékinian, P. Stoffers, D. Ackermand, S. Révillon, M. Maia, M. Bohn, Ridge–hotspot interactions: the Pacific–Ant- arctic Ridge and the Foundation Seamounts, Mar. Geol. 160 (1999) 199 – 223.
[28] C. Hieronymus, D. Bercovicci, Non-hotspot formation of volcanic chains: control of tectonic and flexural stresses on magma transport, Earth Planet. Sci. Lett. 181 (2000) 539 – 557.
[29] M. Mandea, S. Macmillan, T. Bondar, V. Golovkov, B. Langlais, F. Lowes, N. Olsen, J. Quinn, T. Sabaka, International geomagnetic reference field—2000, EOS Trans. Amer. Geophys. Union 82 (2001) 347.
[30] R.L. Parker, The rapid calculation of potential anomalies, Geophys. J. R. Astron. Soc. 31 (1972) 447 – 455.
[31] B.K. Bhattacharya, M.E. Navolio, A fast Fourier transform method for rapid computation of gravity and magnetic anomalies due to arbitrary bodies, Geophys. Prospect. 24
(1976) 633 – 649.
[32] R.J. Blakely, Potential theory in gravity and magnetic applications, Cambridge University Press, Cambridge, UK, 1995.
[33] B.E. Parsons, J.G. Sclater, An analysis of the variation of ocean floor bathymetry and heat flow with age, J. Geophys. Res. 82 (1977) 803 – 827.
[34] J. Dyment, J. Arkani-Hamed, Spreading rate dependent magnetization of the oceanic lithosphere inferred from the anomalous skewness of marine magnetic anomalies, Geophys. J. Int. 121 (1995) 789 – 804.
[35] M. Ravilly, J. Dyment, P. Gente, R. Thibaud, Axial magnetic anomaly amplitude along the Mid-Atlantic Ridge between 20°N and 40°N, J. Geophys. Res. 103 (1998) 24201 – 24222.
[36] S.C. Cande, D.V. Kent, Revised calibration of the geomagnetic polarity time scale for the Late Cretaceous and Cenozoic, J. Geophys. Res. 100 (1995) 6093 – 6095.
[37] D.J. Dunlop, C.J. Hale, Simulation of long-term changes in the magnetic signal of the oceanic crust, Can. J. Earth Sci. 14 (1977) 716 – 744.
[38] U. Bleil, N. Petersen, Variations in magnetization intensity and low-temperature titanomagnetite oxidation of ocean floor basalts, Nature 301 (1983) 384 – 388.
[39] A.L. Wooldridge, S.E. Haggerty, P.A. Rona, C.G.A. Harrison, Magnetic properties and opaque mineralogy of rocks from selected seafloor hydrothermal sites at oceanic ridges,
J. Geophys. Res. 95 (1990) 12351 – 12374.

[40] T. Furuta, Magnetic properties and ferromagnetic mineralogy of oceanic basalts, Geophys. J. Int. 113 (1993) 95 – 114.
[41] H.P. Johnson, J.E. Pariso, Variations in oceanic crustal magnetization: systematic changes in the last 160 million years, J. Geophys. Res. 98 (1993) 435 – 445.
[42] K.C. Macdonald, Near-bottom magnetic anomalies, asymmetric spreading, oblique spreading, and tectonics of the Mid-Atlantic Ridge near lat 378N, Geol. Soc. Amer. Bull. 88 (1977) 541 – 555.
[43] C.A. Raymond, J.L. LaBrecque, Magnetization of the oceanic crust: thermoremanent magnetization or chemical remanent magnetization? J. Geophys. Res. 92 (1987) 8077 – 8088.
[44] E. Geiss, N. Petersen, U. Bleil, Amplitude variation of marine magnetic anomalies, Geol. Rundsch. 78 (1989) 741 – 752.
[45] A. Hildenbrand, P.-Y. Gillot, I. Le Roy, Volcano-tectonic and geochemical evolution of an oceanic intra-plate volcano: Tahiti–Nui (French Polynesia), Earth Planet. Sci. Lett. 217 (2004) 349 – 365.
[46] A. Gripp, R. Gordon, Current plate velocities relative to the hotspots incorporating the NUVEL-1 global plate motion model, Geophys. Res. Lett. 17 (1990) 1109 – 1112.
[47] A. Gripp, R. Gordon, Young tracks of hotspots and current plate velocities, Geophys. J. Int. 150 (2002) 321 – 361.
[48] M. Maia, and the Foundation Hotline Scientific Party, The Foundation Hotspot–Pacific Antarctic ridge interaction: a case study of a ridge approaching a hotspot, Mar. Geol. 167 (2000) 61 – 84.
[49] P. Wessel, W.H.F. Smith, Free software helps map and display data, EOS Trans AGU 72 (441) (1991) 445 – 446.

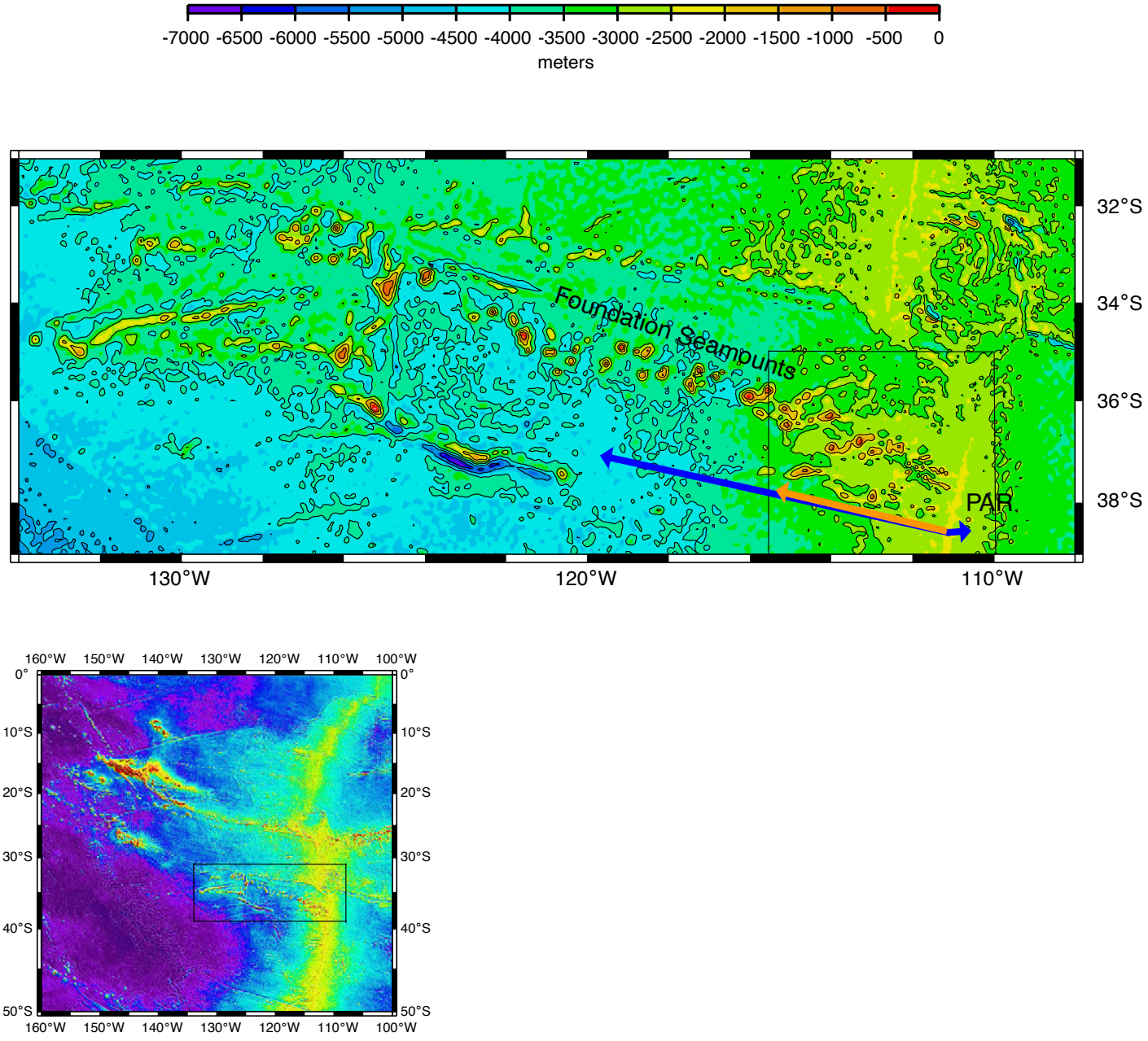

Fig. 1. Top: "Predicted" bathymetry [23] showing the volcanoes of the Foundation chain. The study area is the eastern part of the chain, close to the Pacific–Antarctic Ridge axis, near 110°W. The orange arrow shows the ridge motion on the hotspot reference frame and the blue arrows the absolute motions of the Pacific and the Antarctic plates. Bottom: "Predicted" bathymetry [23] of the South Pacific showing the location of the Foundation chain between the Pacific–Antarctic Ridge and the Austral chain.

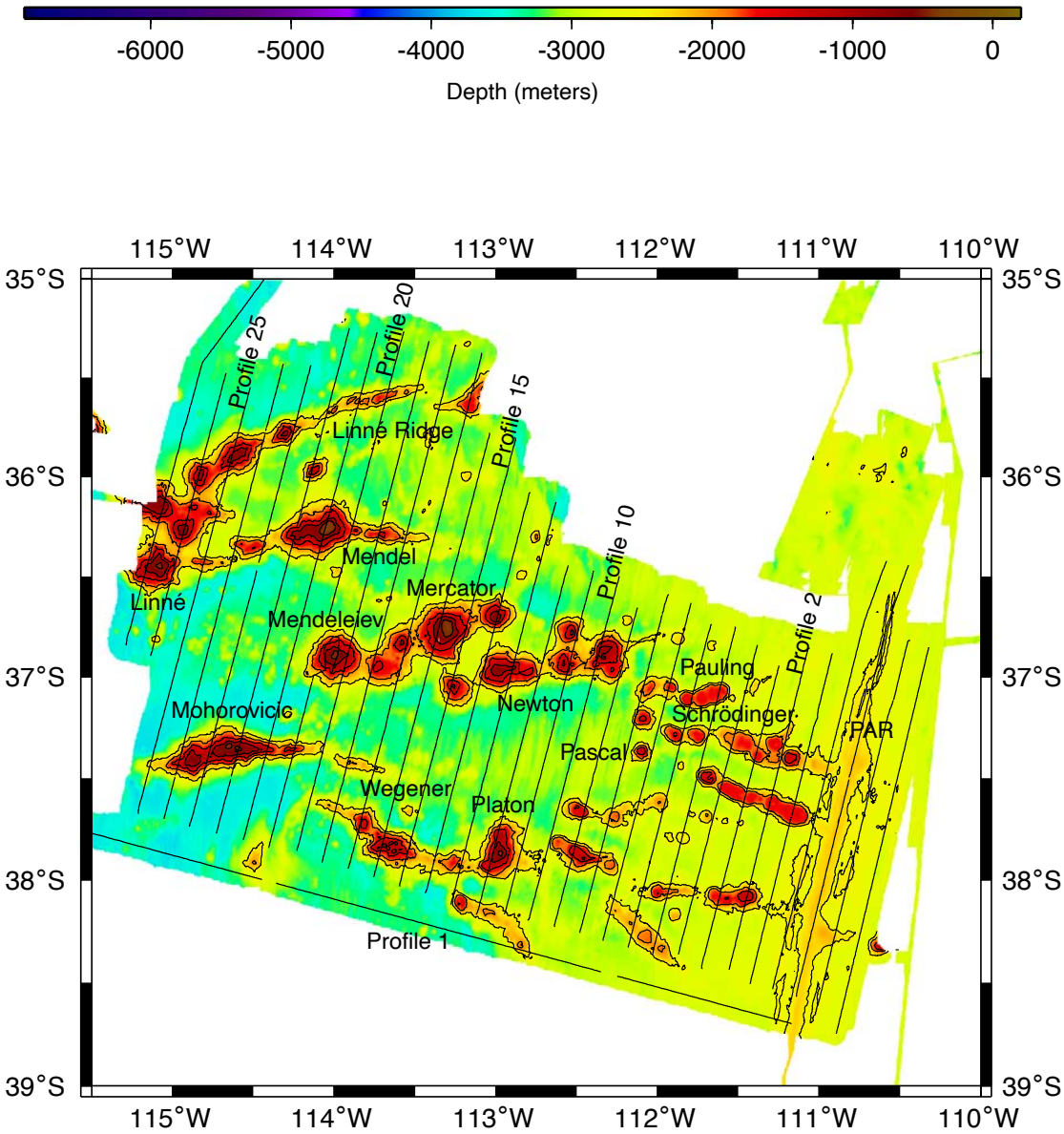

Fig. 2. Multibeam bathymetry grid of the eastern end of the Foundation chain and the Pacific–Antarctic Ridge (PAR) axis. The thin black lines show the location of the magnetic profiles shown in Fig. 7. For clarity only Profiles 1, 2, 10, 15, 20 and 25 are labeled. Profiles east of Profile 2 surveyed the PAR and are not used for the magnetic models. Profile 1 corresponds to a flow line. Labels indicate the location of volcanoes discussed in the text.

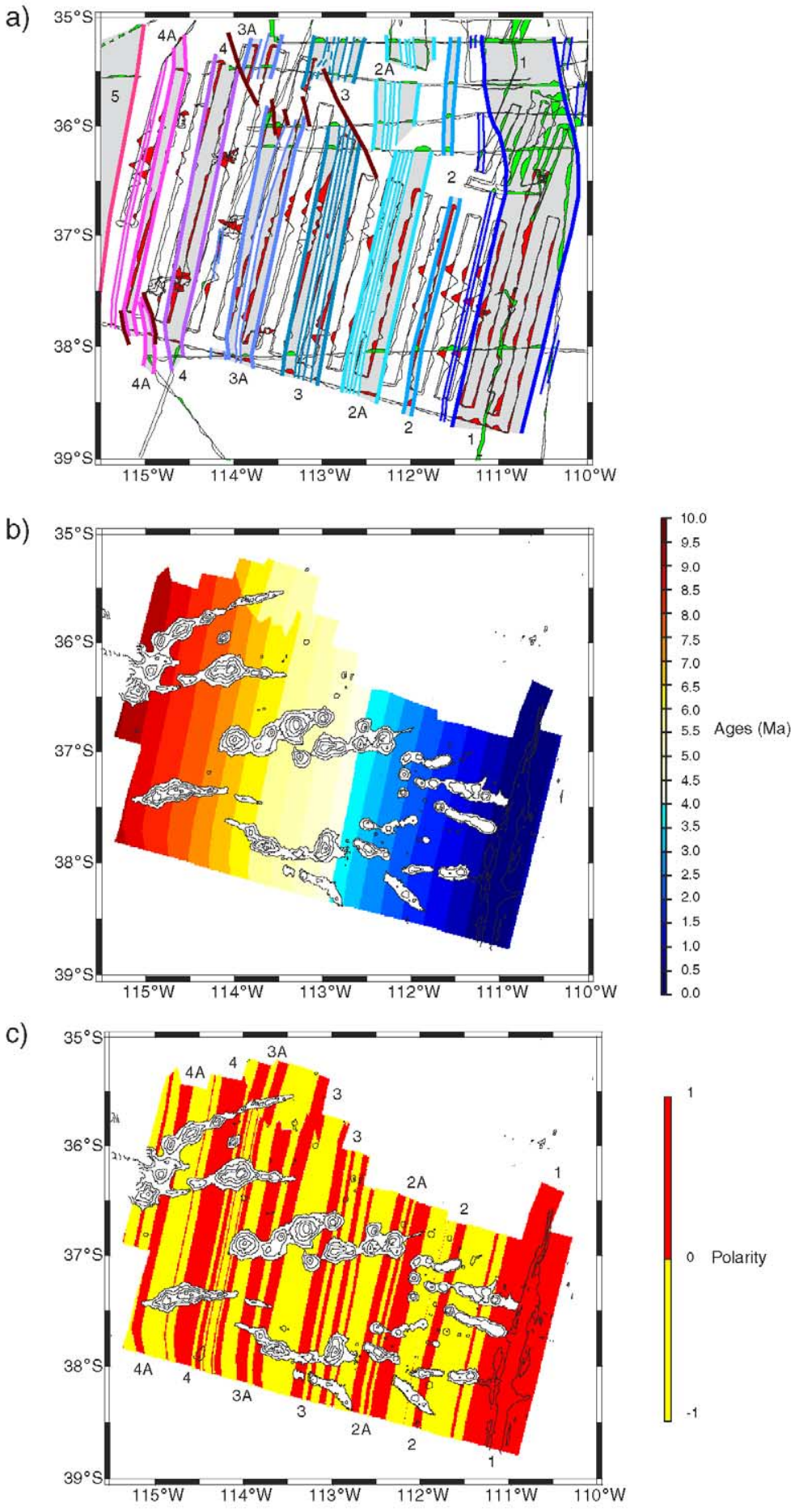
a)
b)
c)
35°S
36°S
37°S
38°S
39°S
115°W
114°W
113°W
112°W
111°W
110°W
5
4A
4
3A
3
2A
2
1
10.0
9.5
9.0
8.5
8.0
7.5
7.0
6.5
6.0
5.5
5.0
4.5
4.0
3.5
3.0
2.5
2.0
1.5
1.0
0.5
0.0
Ages (Ma)
1
0
-1
Polarity

Fig. 3. (a) Magnetic anomaly profiles projected along ship tracks (positive to the west) and interpretation in terms of the age of the underlying oceanic crust. Positive anomalies are plotted in red (data from R/V *L'Atalante* Foundation Cruise) or green (other data), the normally magnetized crust in gray, limited by main and secondary isochrons marked by thick and thin colored lines, respectively, and their associated labels. (b) Age grid of the oceanic crust, computed by using the isochron identifications. (c) Modeled magnetization polarity of the oceanic crust derived from the age grid using Cande and Kent [36] geomagnetic polarity time scale. Red and yellow colors depict normal and reverse polarity, respectively.

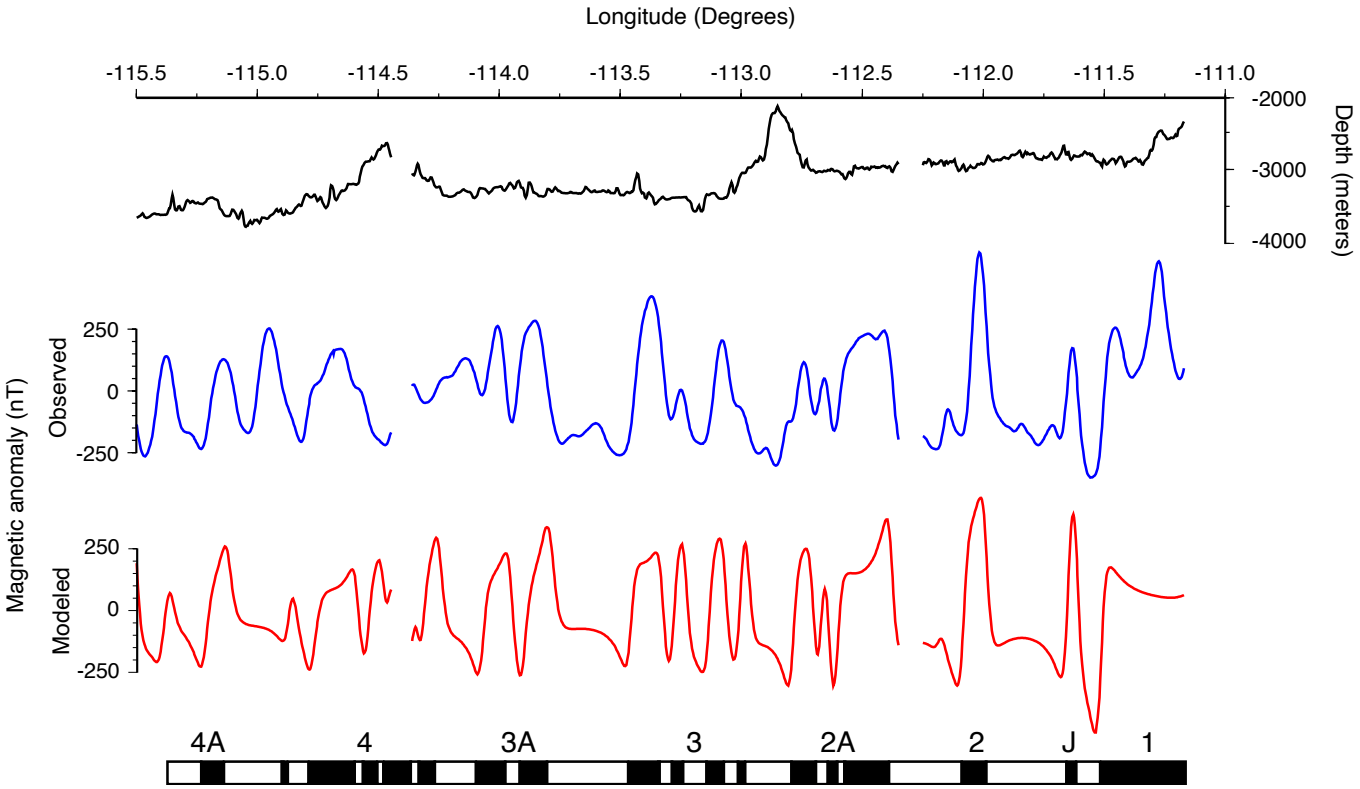

Fig. 4. Comparison between observed (blue line) and modeled (red line) seafloor spreading crustal magnetic anomalies along Profile 1 (see Fig. 2 for location). The corresponding bathymetry is shown in black. The magnetic polarity sequence used to compute the anomalies is also shown. The 3D model used to compute the anomalies is shown in Fig. 3c. Black and white correspond to normal and reverse polarity, respectively.

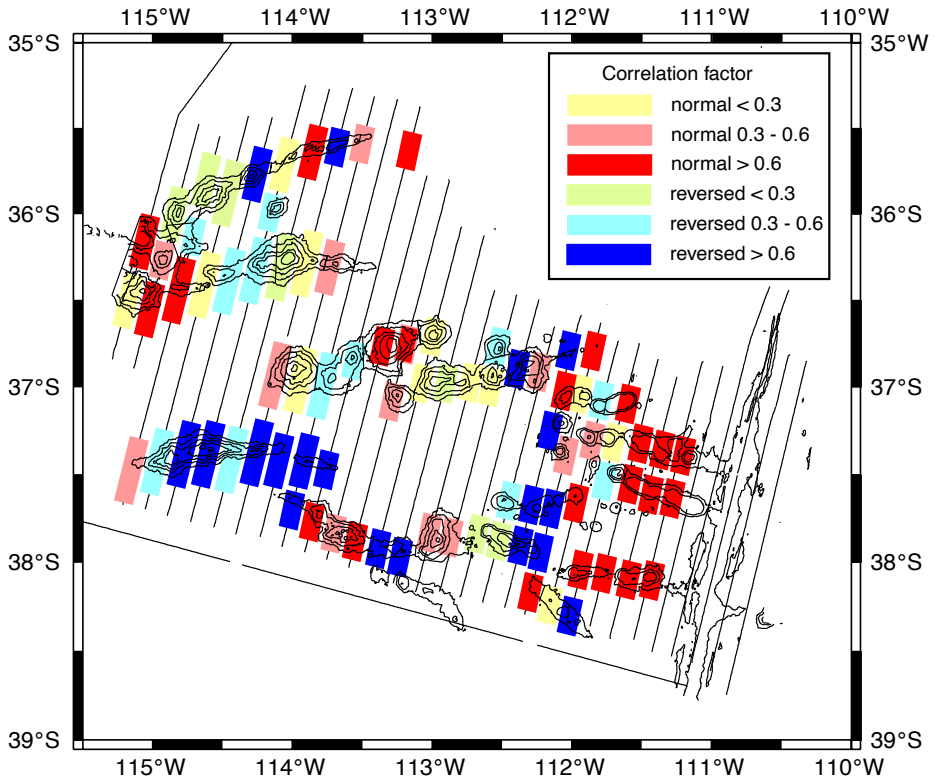

Fig. 5. Correlation coefficients between observed and modeled anomalies. The correlation was computed over each separate volcano. The correlation is considered good for values above 0.6, reasonable for values between 0.3 and 0.6 and poor below 0.3. In the latter case, no choice is made between normal or reverse polarity.

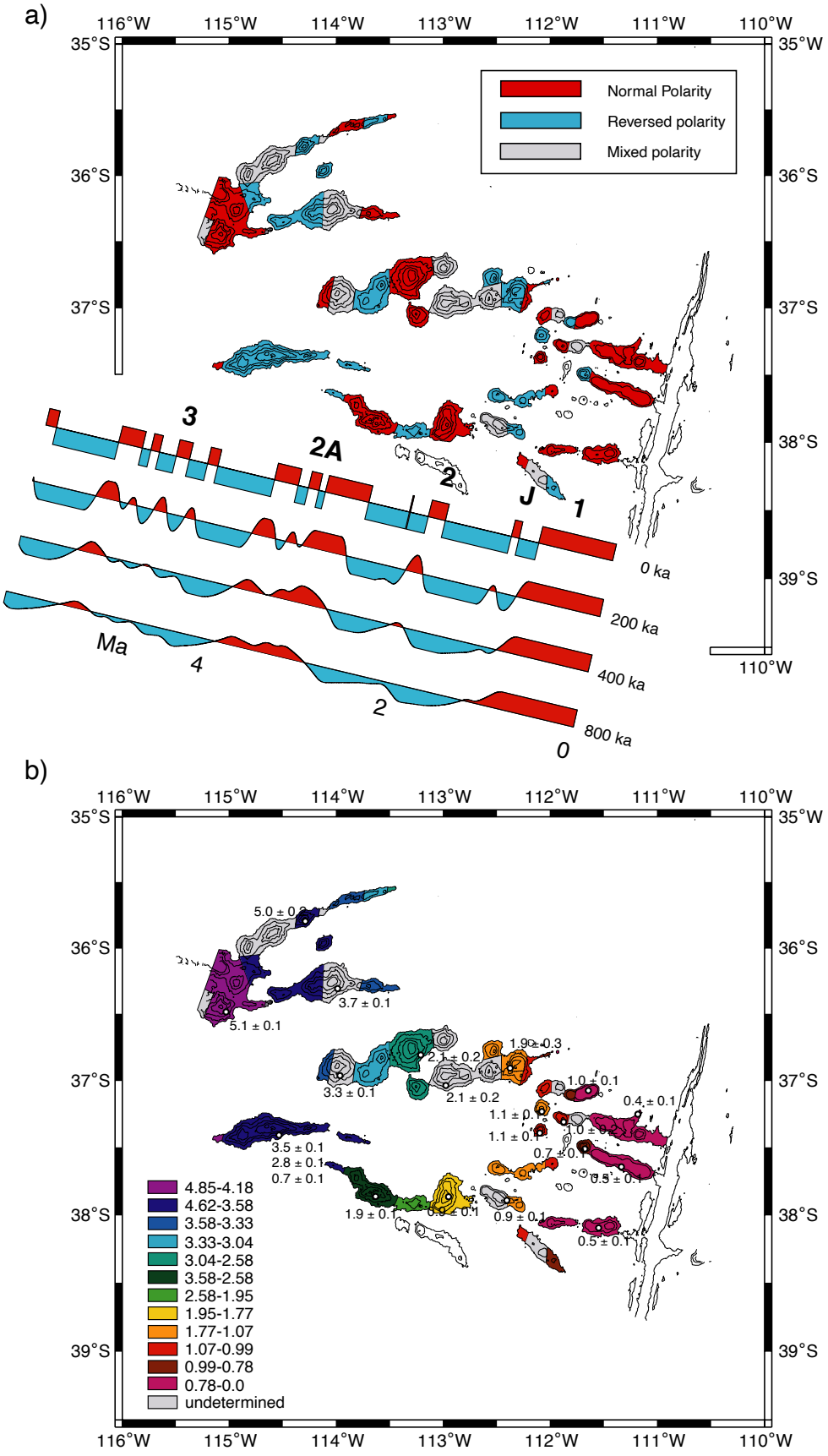
a)
116°W
115°W
114°W
113°W
112°W
111°W
110°W
35°S
36°S
37°S
38°S
39°S
Normal Polarity
Reversed polarity
Mixed polarity
3
2A
2
J
1
0 ka
200 ka
400 ka
800 ka
Ma
4
2
0
b)
4.85-4.18
4.62-3.58
3.58-3.33
3.33-3.04
3.04-2.58
3.58-2.58
2.58-1.95
1.95-1.77
1.77-1.07
1.07-0.99
0.99-0.78
0.78-0.0
undetermined
5.0 ± 0.2
3.7 ± 0.1
5.1 ± 0.1
3.3 ± 0.1
2.1 ± 0.2
1.9 ± 0.3
1.0 ± 0.1
0.4 ± 0.1
1.1 ± 0.1
0.7 ± 0.1
3.5 ± 0.1
2.8 ± 0.1
0.7 ± 0.1
1.9 ± 0.1
0.9 ± 0.1
0.5 ± 0.1

Fig. 6. (a) Final magnetic model showing volcanoes conveniently modeled with a reverse polarity, in blue, and a normal polarity, in red. The edifices where no clear polarity could be identified are depicted in gray and correspond to the shaded areas of Fig. 7. The polarity sequence is represented at the bottom with, from top to bottom, the original sequence (marked 0 ka) and the same after convolution with filters simulating the duration of volcano construction (Fig. 8), respectively, 200, 400 and 800 ka long. (b)Ages of the volcanoes derived from the magnetic models (colors). Radiometric ages available for the volcanoes are displayed near the dredge locations, indicated by black circles.

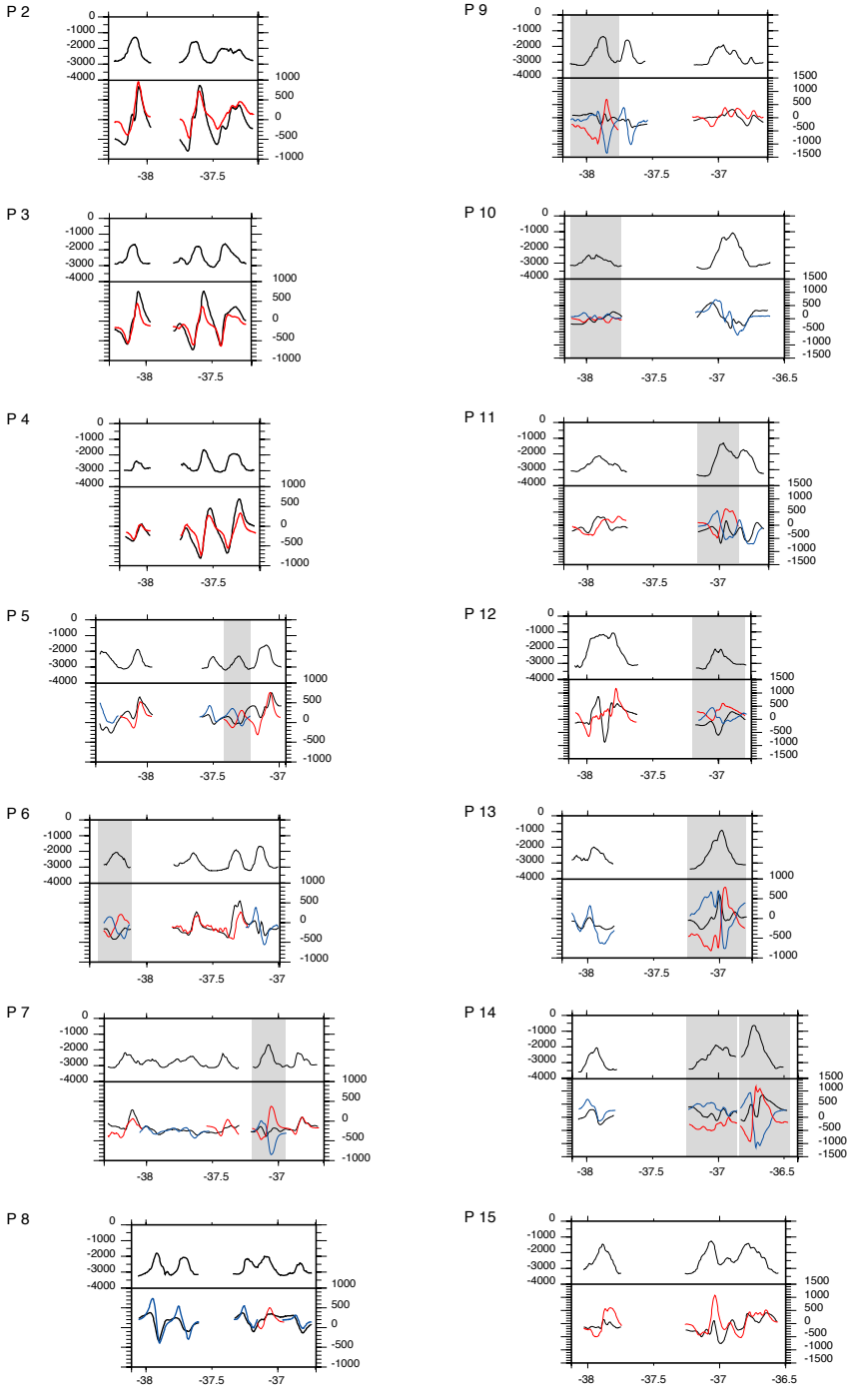

Fig. 7. Bathymetry (top) and magnetic anomaly (bottom) profiles across the volcanoes of the Foundation Chain. The observed magnetic anomaly (with the effect of the underlying oceanic crust removed) is shown in black. The red and blue lines represent modeled anomalies using normal and reverse polarities, respectively. Shades depict areas where the fit is of too poor quality to discriminate between the two models. See Fig. 2 for profile location.

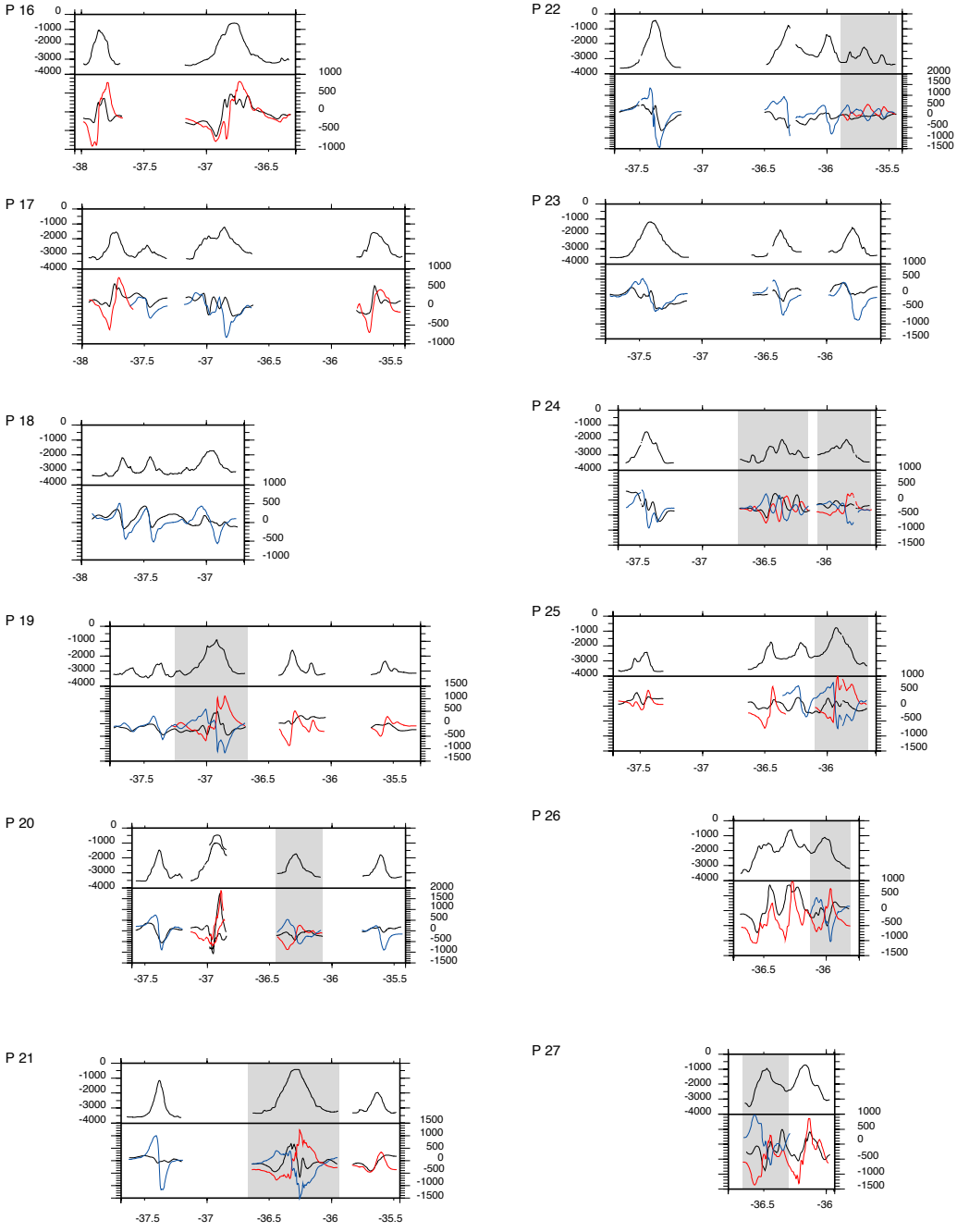

Fig. 7 (*continued*).

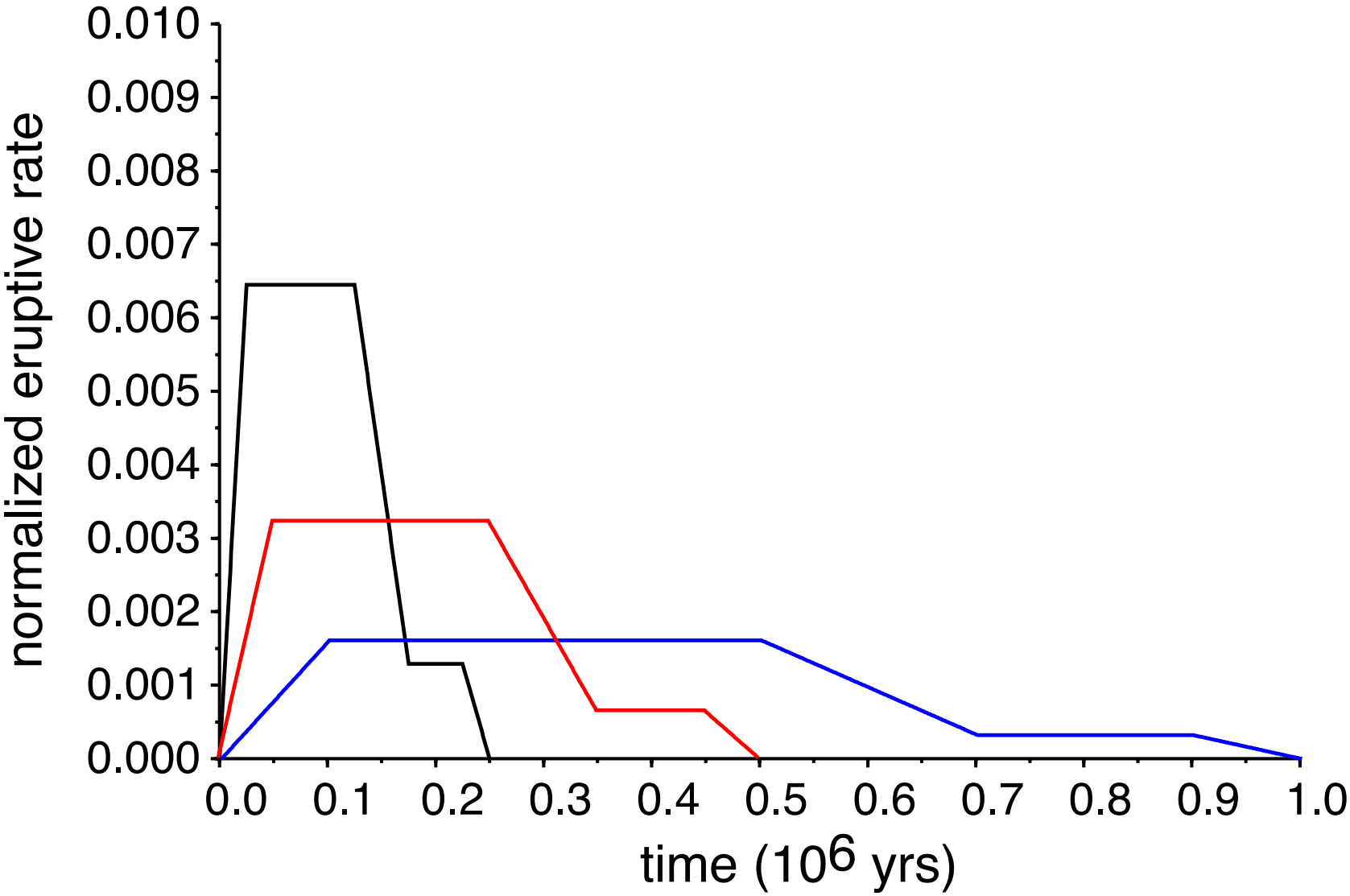

Fig. 8. Filters simulating the building of an intraplate volcano for a short (black line: 200 ka), medium (red line: 400 ka) and long (blue line: 800 ka) constructional phase. The eruptive rates is normalized before convolution in order to insure that its integral is 1.

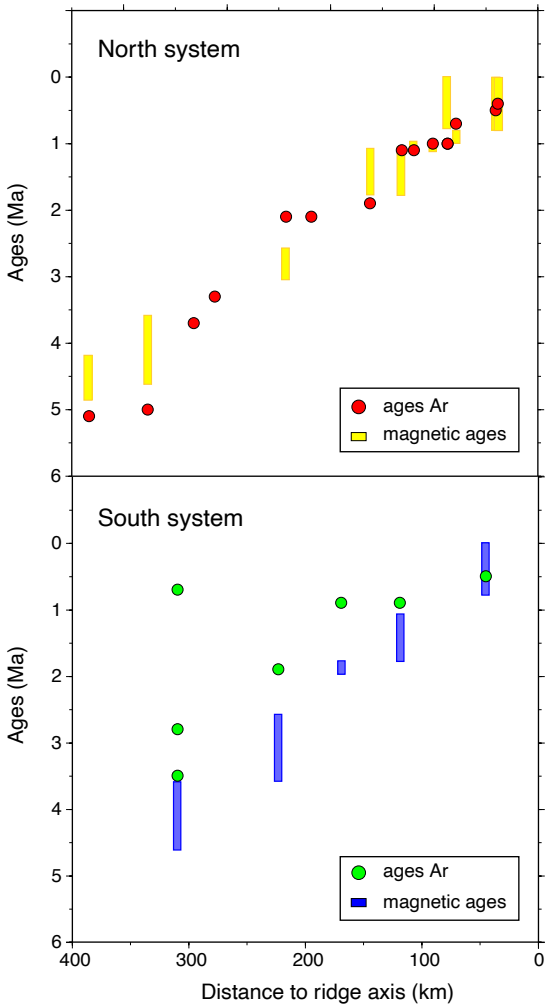

Fig. 9. Comparison between the magnetic ages (rectangles) and the radiometric argon ages (circles). Data for the North system are represented by red circles for argon radiometric ages and yellow rectangles for magnetic age intervals. Data for the South system are represented by green circles for argon radiometric ages and dark blue rectangles for magnetic age intervals.

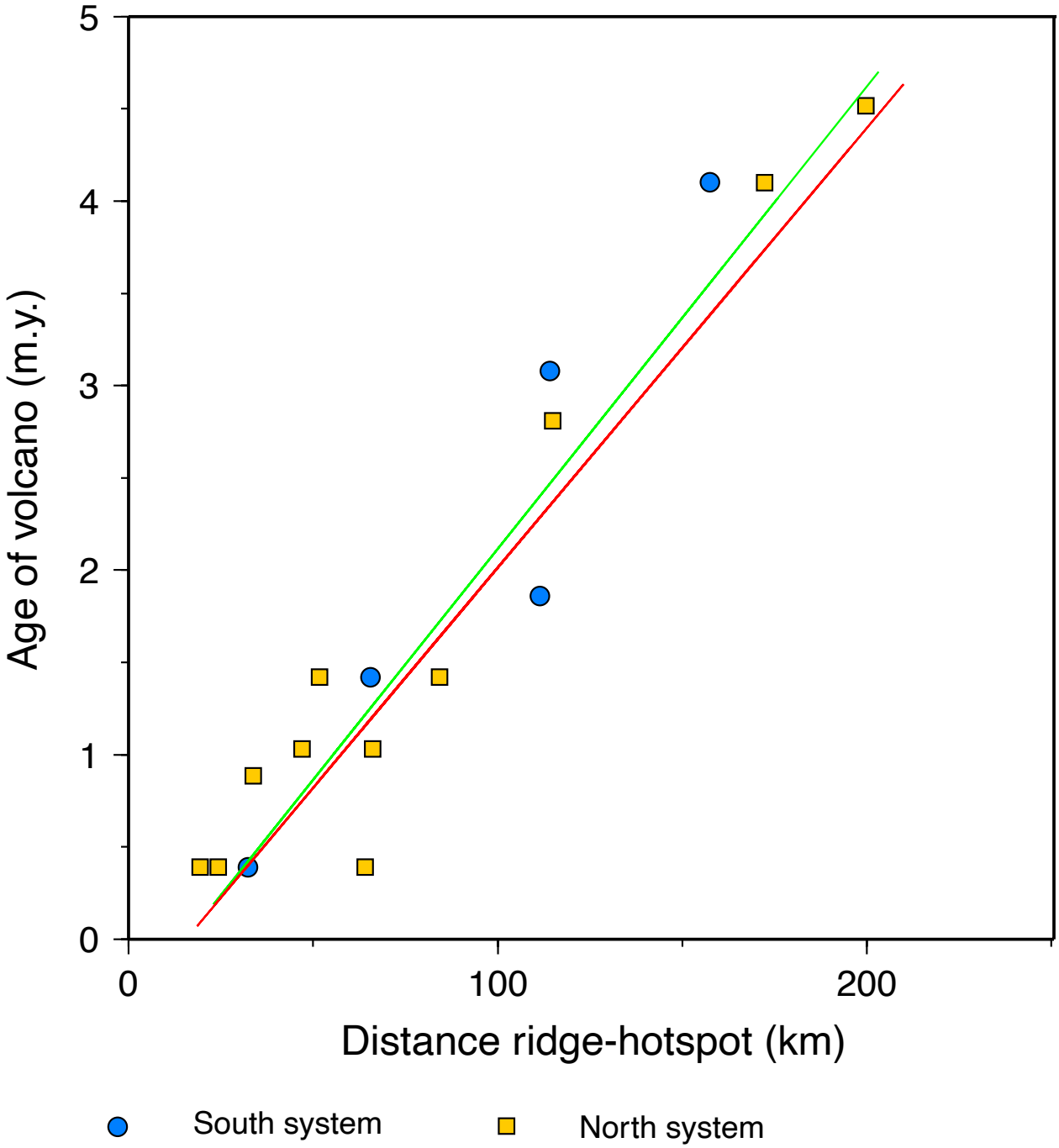

Fig. 10. Plot of the average ages of the volcanoes derived from the magnetic modeling as a function of the distance between the ridge and the hotspot. The red line represents the relative motion of the Pacific Antarctic Ridge with respect to the hotspot derived from the absolute plate motion model (rate of 43 km/Ma) and the green line the best fitting line for the entire data set (rate of 40 km/Ma, present distance of 20 km).